A Comparative Study of Recent Multi-Component Unmixing Algorithms

Zhang Mo and Stéphane Pezeril

A COMPARATIVE STUDY OF RECENT MULTI-COMPONENT UNMIXING ALGORITHMS

Mo Zhang , Stéphane Pezeril

Innovation & Research center of AUSY Group, Sèvres, France

ABSTRACT

In this paper, we consider the problem of blind multicomponent image unmixing. Two mixing models are considered : the linear mixing model (LMM) and its extended version (ELMM) which take the spectral (i.e. endmember) variability into account. We introduce powerful unmixing algorithms utilizing these models of latest state-of-the-art, and compare their performance on endmember recovery and abundance estimation.

Index Terms— spectral unmixing, multispectral image, hyperspectral image, evaluation assessment

1. INTRODUCTION

Due to limited spatial resolution, the pixel of multicomponent images acquired by multicomponent (multi- or hyper-spectral) remote sensing systems (mounted on satellite, airborne or UAV platforms) is often a mixture of diffrent materials. Spectral unmixing aims at identifying the group of spectral signatures representing the constitutional materials (called endmembers) and estimating their corresponding proportions (called abundances) in every pixel.

Depending on the mixing situation within every pixel, there exists two kinds of mixture model : linear and nonlinear [1]. The linear mixing model (LMM) assumes that the spectrum of each pixel is composed by a linear combination of endmembers weighted by their corresponding abundances [2]. However, in real scenarios, the mixture of endmembers could not always be described as linear (by reason of intimate mixing effects or multiple scattering etc.). The nonlinear model is thus introduced (a review can be found in [3]).In this paper, we will be focused in the approaches utilizing the linear model.

A big drawback of LMM is that it undertakes every endmember could be properly represented by a single spectrum, which is unfortunately not always true in real life scenarios as there always exists an intra-class variability whthin each material. The spectral variability could be caused by multiple factors such as the variation of illumination conditions, the intrinsic variability of the materials and the topography of the imaged scene [4]. In the litterature, the spectral variability could be modeled by some probability distributions [5]. The endmembers are assumed to follow Gaussian, Beta or other parametric distributions. However, the choice of distribution model, which is considered as prior information, is empirical and varies from one multicomponent image to another. Another possibility to model the endmember variability is to use a collection of samples from a given spectral signature, the samples are called spectral bundles [6]. The variability is considered implicitly in this way but this strategy requires existence of at least one pure pixel for each endmember.

Recently, the sepctral variability has been held by using extended linear mixing model (ELMM) [7]. The main advantage of this strategy is about preserving the framework of LMM.
Both of the models (LMM and ELMM) have created plenty of spectral unmixing approaches.

In this paper, we present a large-scale comparison between the unmixing algorithms employing the two mixing models described above. In the case of LMM, we will analyse the approache Spatial Group Sparsity Regularized Nonnegative Matrix Factorization (SGSNMF)[8], Rank-Deficient Non Negative Matrix Factorization (RDNMF) [9], Minimum volume (3 types of regularisation) Non Negative Matrix Factorization (MVNMF) [10], Minimum volume (3 types of regularisation) Non Negative Matrix Factorization with Parameter Selection (MV-PSNMF) [11] and Collaborative Nonnegative Matrix Factorization (3 types of regularisation) (CONMF) [12]. In the case of ELMM, we will study the behavior of the approaches using ELMM and its vairations : the approache employing ELMM [7] and the approache using Generalized linear mixing model (GLMM) [13].

This paper aims at analysing the performance of the aforementioned algorithms in respect of accuracy criteria and robustness to the noise. Different multicomponent (hyper/multi-spectral) images, simulated or the real ones, have been used to evaluate the unmixing approaches.

The structure of the paper is organized as follows :
Sect. 2 consists of a breif review of the above-mentioned unmixing approaches. Sect. 3 describes the test images and the criteria utilized to evaluate the approaches. The experiment results are discussed in Sect. 4 and finally, we present the conclusion of the paper in Sect. 5

2. REVIEW OF RELATED WORK

2.1. LMM

In the case of LMM, suppose that we have the mixing model as follows :

$$Y = SA + \varepsilon.$$

where $Y \in R^{L \times N}$ represents the multicomponent image whithin L the number of spectral bands and N the total number of pixels; $S \in R^{L \times p}$ is the matrix of endmembers with P the number of materials; $A \in R^{p \times N}$ corresponds to the abundances fractions of S *and* $\varepsilon \in R^{L \times N}$ represents the noise and other estimation errors. The unmixing process can be formulated by an constrained optimization problem as :

$$C(S,A) = \|Y - SA\|_2^2 + \beta_S \times Reg(S) + \beta_A \times Reg(A)$$
$$s.c.\ S \geq 0 \text{ and } \sum a_{i,j} = 1$$

where $\|Y - SA\|_2^2$ represents the data fitting term, the Frobenius norm is the most used model, other forms of like beta-divergence could be found in [14] . In this study, we will focus only on the Frobenius norm. The term $Reg()$ corresponds to the regularization of S (resp A) and β_S (resp β_A) is the associated hyper-parameter. $a_{i,j}$ represents the (i,j)th element of matrix A within i∈{1..L} and $j \in \{1..N\}$.The endmembers must respect the non-negativity constraint and the abundances should take the rule "sum-to-one" into account.

In SGSNMF [8], the authors proposed to introduce a group-structured prior information of the image in assuming that the pixels of a local spatial group (named by « superpixel ») share the same sparse structure in the abundance matrix. The estimation is thereby achieved by the level of superpixel. The proposed novel regularisation of A is given by :

$$Reg(A) = \sum_{g=1}^{G} \sum_{q \in \Theta_g} c_q \left\| W_g \alpha_q \right\|_2$$

where θ_g is the gth super-pixel; $a_q \in R^{N_g}$, abundance of the qth pixel in θ_g, within N_g the number of the pixels in θ_g; $W_g \in R^{p \times p}$ the weighted matrix and c_q represents a pixel-wised coefficient defined by $c_q = \frac{1}{D_q^g}$ with D_q^g measures the spectra-spatial distance between qth pixel and the centroid of θ_g.

Other researchers tried to impose the regularization on the endmember. The most famous regularization corresponds to the minimum volume one. The proposition of a such regularization is inspired by the assumption that the endmembers of a multicomponent image are vertices of a minimum volume enclosing all of its pixels [15]. In CONMF [12], the authors have introduced three minimum-volume based regularisations named respectively by CONMF-VCA, CONMF-centerd and CONMF-total variance. All of them are formulated in the quadratic form as below :

$$Reg(S) = \|BS\text{-}O\|_2^2$$

where {B, O} is a set of parameters defining the regularization. In the case of CONMF-VCA, $B = I_p$ and $O =$ estimation of endmembers obtained by the method vertex component analysis [16] where I_p represents the identity matrix. In the case of CONMF-centerd, $B = I_p$ and $O = \bar{Y}$ where $\bar{Y} = \frac{1}{N}\sum y$ is the mean value of the data set. Finally, in the case of CONMF-total variance, $B = I_p - (\frac{1}{p})1_p 1_p^T$ and $O = 0$. In addition to impose the regularisation on S, the authors of [12] proposed a mixed-norm type regularizer on A which is given by : $\|A\|_{2,1} = \sum \|a_{i,}\|_2$ where $a_{i,}$ represents the ith row of the matrix A. In [12], the regularizer $\|A\|_{2,1}$ is used as well to estimate the number of endmembers : the criteria $\|a_{i,}\|_2$ is considered to mesure the sparseness of each row in abundances matrix and $\|a_{i,}\|_2 = 0$ if the ith endmember dosen't exist. The approach MV-PSNMF proposed in [11] used the same regularizer on S as [12], noted respectively by MV-PSNMF-VCA, MV-PSNMF-centered and MV-PSNMF-total variance. The main diffrence between the two approaches lies in the choice of hyperparameter β_S : Instead of fixing an empirical value as done

in [12], the authors of MV-PSNMF proposed to determine the value by minimizing the distance between the border pixels (obtained by method proposed in [17]) and the hyperplan generated by the estimated endmembers. In method MVNMF [10], the authors utilised the minimum-volume based regularizers as well. Different from the quadratic ones introduced previously, the three volume regularisations used in the approach are based on the determinant of the Gramian matrix of S :

MVNMF-det : $Reg(S) = \det(S^T S)$
MVNMF-logdet : $Reg(S) = \log[\det(S^T S + \delta I)]$
MVNMF-nuclear : $Reg(S) = \|S\|_*$

Finally, the method RDNMF proposed in [9] takes the regularizer of MVNMF-logdet. A special situation is considered here : when the number of spectral bands is fewer than that of endmembers (i.e. L<p).

2.2. ELMM

The method ELMM presented in [7] consists of minimising a cost function as follows :

$$\underset{A\in\triangle_K,S,\varphi,S_0}{\text{MIN}} \frac{1}{2}\sum_{n=1}^{N}(\|y_n - a_n S_n\|_2^2 + \beta_S\|S_n - \varphi_n S_0\|_F^2)$$
$$+ \beta_A\|\nabla A\|_{2,1} + I_{R_+^{K\times P}}(A) + \mu^T(A^T 1_K - 1_P)$$
$$+ \frac{\beta_\varphi}{2}\|\nabla\varphi\|_F^2$$

where $S = \{\mathbf{S_n}\} \in R^{L\times P\times K}$, and $A \in \triangle_K$ implies that each abundance vector $a_p \in R^K$ belongs to a unity simplex of K vertices. $\varphi_p \in R^{K\times K}$ is a diagonal matrix of scale factors. $\mathbf{S_0}$ corresponds to a reference endmember matrix. $\mu \in R^P$ is the multiplier of the lagrange. The authors of GLMM [13] tried to generalise ELMM in replacing φ by a three-dimensional scaling tensor such that $\varphi \in R^{L\times p\times N}$. GLMM aims at affecting unevenly different wavelength intervals so that some complicated spectral perturbations could be taken into account.

3. TEST IMAGES AND EVALUATION ASSESEMENTS

This section shows different simulated/real multicomponent images and evaluation criteria used to achieve the comparison among the 13 aforementioned unmixing methods.

3.1. Synthetic and real data

In the tests with simulated data, we consider both multispectral (L=12) and hyperspectral cases (L=30). The simulated images are generated by LMM and all of them comprise 256x256 pixels.
To simulate the synthetic images, we used the spectral signatures from the United States Geological Survey (USGS) spectral library released in 2007 [18]. The abundance maps are generated by the

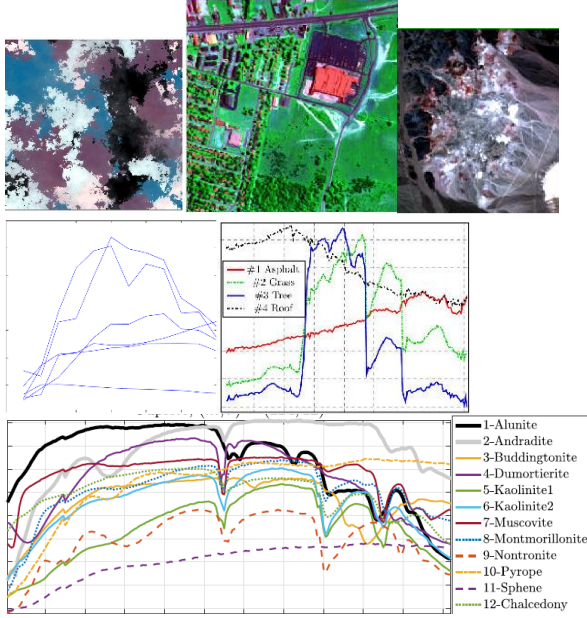Dirichlet distribution method [19]. In the multispectral case, 4 test

Fig1 : 1ʳᵗ line from left to right, simulated image with p=6 ; Urban ;Cuprite
2ⁿᵈ line from left to right : the corresponding spectral signature

images are simulated whithin respectively 3,6,12 and 15 endmembers while 2 hypserspectral images are generated with corresponding 5 and 20 endmembers. In each pixel of the simulated image, the maximal number of endmembers comprised is set to 3 when p=3 and set to 5 for other cases. Finally, we make the maximal abundance fraction 0.8 so that no pure pixels would be present in the test images. For each of the simulated image, we add the zero-mean Gaussian noise of 3 levels (20,30 and 40dB) using Signal-to-Noise Ratio (SNR). Two real hyperspectral images are used in our comparative study : the first one is the wellknown Airborne Visible Infra-Red Imaging Spectrometer (AVIRIS) Cuprite data set [20]. The image comprise 12 endmembers and 188 spectral bands after a remouvement of the water absorption and the noisy ones. We take a subset of 250x191 in our experiments. The second real image corresponds to the famous Urban data set within 4 endmembers. There are 307x307 pixels and 162 spectral bands after remouvement. The reference spectral signatures and/or abundance maps are downloaded from the website as below :

http://lesun.weebly.com/hyperspectral-data-set.html
Fig 1 shows some of the tested images in RGB version with their corresponding spectral signals.

3.2. Performance metrics

We measure the quality of the estimated endmember $\hat{S}$ by spectral angle distance (SAD) in degree as : $cos^{-1}\left[\frac{\langle s,\hat{s}\rangle}{\|s\|\|\hat{s}\|}\right]$

The recovered abundance map $\hat{A}$ will be compared with its reference through a Manhattan distance based criteria :

$$\|A - \hat{A}\|_1$$

4. EXPERIMENT RESULTS

For all of the experiments, we assume that the number of endmembers *P* is known and the other parameters (hyperparameters number of iterations and other parameters involved in optimisation process) are set as proposed by the authors. Moreover, we note that the endmembers estimated by the methods using ELMM could not be evaluated due to the spectral variability (the size of S and $\hat{S}$ are not same)

4.1. Using the simulated data

4.1.1. Estimation of S

In TABLE I, we show the the name of the approach (based on LMM) which achieved the minimal value in SAD at each of the test case :

LMM		Best approach in estimation S		
	P	20dB	30dB	40dB
L=12	3	CONMF	MV-PSNMF-VCA and – total variance	CONMF
	6	SGSNMF	SGSNMF	MV-PSNMF-total variance
	12	SGSNMF	MV-PSNMF-VCA and – total variance	SGSNMF
	15	RDNMF		
	p	20dB	30dB	40dB
L=30	5	MV-PSNMF-centered	MV-PSNMF-total variance	MV-PSNMF-total variance
	20	SGSNMF		

TABLE I

4.1.2. Estimation of A

In TABLE II, we introduce the name of the approach based on LMM which achieved the best value through Mahattan distance at each of the test case :

LMM		Best approach in estimation A		
	P	20dB	30dB	40dB
L=12	3	MV-PSNMF-total variance	MV-PSNMF-total variance	MV-PSNMF-total variance
	6	SGSNMF	SGSNMF	MV-PSNMF-total variance
	12	SGSNMF		
	15	RDNMF		
	p	20dB	30dB	40dB
L=30	5	MV-PSNMF-total variance	SGSNMF	MV-PSNMF-total variance
	20	SGSNMF		

TABLE II

Among the ELMM-based approaches, the method GLMM outperformed ELMM in all of the experiments. Finally, we tried to compare the performance of GLMM with the best LMM based method. We present in TABLE III the most powerful algorithm in recovery of abundance maps :

LMM and ELMM		Best approach in estimation A		
	P	20dB	30dB	40dB
L=12	3	GLMM	GLMM	MV-PSNMF-total variance
	6	GLMM		
	12	GLMM	SGSNMF	GLMM
	15	RDNMF		
	p	20dB	30dB	40dB
L=30	5	GLMM		
	20	SGSNMF	SGSNMF	SGSNMF

TABLE III

The results presented in TABLE I, II and III show the following :

- Among the LMM based algorithms, the approach SGSNMF and the MV-PSNMF based ones (especially VCA and total variance versions) showed a better performance on estimation of S and A in most of the test cases and they are robust to different levels of noise.
- In both multispectral and hyperspectral tests, the MV-PSNMF based algorithms performed better when the number of endmembers is lower while SGSNMF outperformed all other LMM based methods in most of the cases when the value of P is larger.
- The methode RDNMF is the only one who can handle the case where P>L, which means S is rank-deficient. However, its performance is poor in other full rank test cases.
- The ELMM based method GLMM outeperformed most of the LMM based ones in recovery of A when the value of P is small but it's poorer than SGSNMF when P is larger.

4.2. Using the real data

In TABLE IV and V, we show respectively the first three efficient methods in recovery of true S and A. We do not present the recovery of A in Cuprite case as we didn't get its abundance map reference.

LMM and ELMM		Top 3 approaches in estimation S		
	P	Top1	2	3
Urban L=162	4	MVNMF-det	SGSNMF	MV-PSNMF-total variance
Cuprite L=188	12	SGSNMF	MVNMF-det	MVNMF-nuclear

TABLE IV

LMM and ELMM		Top 3 approaches in estimation A		
	P	Top1	2	3
Urban L=162	4	GLMM	MV-PSNMF-total variance	SGSNMF

TABLE V

We could see from the two tables above that the method SGSNMF, MV-PSNMF (- total variance version) and GLMM outperformed the other unmixing algorithms in the tests of real hyperspectral images.

5. CONCLUSION

In this paper, we analyzed several recent proposed multicomponent image unmixing algorithms and we tried to compare their performance in estimation of endmembers and abundance fractions. The unmixing methods taking into comparison are divided into two types according to their mixing model : linear mixing model (LMM) and extended linear model (ELMM). Thanks to different experiments using simulated and real data, multispectral and hyperspectral, we found that the LMM based methods SGSNMF and MV-PSNMF (especially the total variance version) performed better in recovery of endmember S than other LMM type methods and they showed a robustness to the noise. In estimation of abundance maps A, the ELMM based method GLMM outperformed all other methods when the number of endmembers is small and SGSNMF is the most efficient one when this number is larger. Moreover, the MV-PSNMF based methods required the less prior information as their regularisation parameter is estimated. MVNMF based methods tried to include a process of estimation of endmember number, however, it's always widely overestimated. Finally, although the methods GLMM and SGSNMF showed a very good performance in estimation of A, they are very time consuming due to the mixing model complexity and the « superpixel » segmentation procedure.

6. REFERENCES

[1]   J. Yu, D. Chen, Y. Lin, et S. Ye, « Comparison of linear and nonlinear spectral unmixing approaches: a case study with multispectral TM imagery », *Int. J. Remote Sens.*, vol. 38, nº 3, p. 773-795, févr. 2017, doi: 10.1080/01431161.2016.1271475.

[2]   C. Quintano, A. Fernández-Manso, Y. E. Shimabukuro, et G. Pereira, « Spectral unmixing », *Int. J. Remote Sens.*, vol. 33, nº 17, p. 5307-5340, sept. 2012, doi: 10.1080/01431161.2012.661095.

[3]   R. Heylen, M. Parente, et P. Gader, « A Review of Nonlinear Hyperspectral Unmixing Methods », *Sel. Top. Appl. Earth Obs. Remote Sens. IEEE J. Of*, vol. 7, p. 1844-1868, juin 2014, doi: 10.1109/JSTARS.2014.2320576.

[4]   A. Zare et K. C. Ho, « Endmember Variability in Hyperspectral Analysis: Addressing Spectral Variability During Spectral Unmixing », *IEEE Signal Process. Mag.*, vol. 31, nº 1, p. 95-104, janv. 2014, doi: 10.1109/MSP.2013.2279177.

[5]   X. Du, A. Zare, P. Gader, et D. Dranishnikov, « Spatial and Spectral Unmixing Using the Beta Compositional Model », *IEEE J. Sel. Top. Appl. Earth Obs. Remote Sens.*, vol. 7, nº 6, p. 1994-2003, juin 2014, doi: 10.1109/JSTARS.2014.2330347.

[6]   B. Somers, M. Zortea, A. Plaza, et G. P. Asner, « Automated Extraction of Image-Based Endmember Bundles for Improved Spectral Unmixing », *IEEE J. Sel. Top. Appl. Earth Obs. Remote Sens.*, vol. 5, nº 2, p. 396-408, avr. 2012, doi: 10.1109/JSTARS.2011.2181340.

[7]   L. Drumetz, M.-A. Veganzones, S. Henrot, R. Phlypo, J. Chanussot, et C. Jutten, « Blind Hyperspectral Unmixing Using an Extended Linear Mixing Model to Address Spectral Variability », *IEEE Trans. Image Process.*, vol. 25, nº 8, p. 3890-3905, août 2016, doi: 10.1109/TIP.2016.2579259.

[8]   X. Wang, Y. Zhong, L. Zhang, et Y. Xu, « Spatial Group Sparsity Regularized Nonnegative Matrix Factorization for Hyperspectral Unmixing », *IEEE Trans. Geosci. Remote Sens.*, vol. 55, nº 11, p. 6287-6304, nov. 2017, doi: 10.1109/TGRS.2017.2724944.

[9]   V. Leplat, A. M. S. Ang, et N. Gillis, « Minimum-volume Rank-deficient Nonnegative Matrix Factorizations », in *ICASSP 2019 - 2019 IEEE International Conference on Acoustics, Speech and Signal Processing (ICASSP)*, mai 2019, p. 3402-3406, doi: 10.1109/ICASSP.2019.8682280.

[10]   A. M. S. Ang et N. Gillis, « Algorithms and Comparisons of Nonnegative Matrix Factorizations With Volume Regularization for Hyperspectral Unmixing », *IEEE J. Sel. Top. Appl. Earth Obs. Remote Sens.*, p. 1-11, 2019, doi: 10.1109/JSTARS.2019.2925098.

[11]   L. Zhuang, C.-H. Lin, M. A. T. Figueiredo, et J. M. Bioucas-Dias, « Regularization Parameter Selection in Minimum Volume Hyperspectral Unmixing », *IEEE Trans. Geosci. Remote Sens.*, vol. 57, nº 12, p. 9858-9877, déc. 2019, doi: 10.1109/TGRS.2019.2929776.

[12]   J. Li, J. M. Bioucas-Dias, A. Plaza, et L. Liu, « Robust Collaborative Nonnegative Matrix Factorization for Hyperspectral Unmixing », *IEEE Trans. Geosci. Remote Sens.*, vol. 54, nº 10, p. 6076-6090, oct. 2016, doi: 10.1109/TGRS.2016.2580702.

[13]   T. Imbiriba, R. A. Borsoi, et J. C. Moreira Bermudez, « Generalized Linear Mixing Model Accounting for Endmember Variability », in *2018 IEEE International Conference on Acoustics, Speech and Signal Processing (ICASSP)*, avr. 2018, p. 1862-1866, doi: 10.1109/ICASSP.2018.8462214.

[14]   V. Leplat, N. Gillis, et C. Févotte, « Multi-Resolution Beta-Divergence NMF for Blind Spectral Unmixing », *ArXiv200703893 Cs Eess*, juill. 2020, Consulté le: oct. 18, 2020. [En ligne]. Disponible sur: http://arxiv.org/abs/2007.03893.

[15]   M. D. Craig, « Minimum-volume transforms for remotely sensed data », *IEEE Trans. Geosci. Remote Sens.*, vol. 32, nº 3, p. 542-552, mai 1994, doi: 10.1109/36.297973.

[16]   J. M. P. Nascimento et J. M. B. Dias, « Vertex component analysis: a fast algorithm to unmix hyperspectral data », *IEEE Trans. Geosci. Remote Sens.*, vol. 43, nº 4, p. 898-910, avr. 2005, doi: 10.1109/TGRS.2005.844293.

[17]   C. B. Barber, D. P. Dobkin, et H. Huhdanpaa, « The quickhull algorithm for convex hulls », *ACM Trans. Math. Softw.*, vol. 22, nº 4, p. 469–483, déc. 1996, doi: 10.1145/235815.235821.

[18]   « Spectroscopy Lab ». https://www.usgs.gov/labs/spec-lab (consulté le oct. 16, 2020).

[19]   T. Minka, « Estimating a Dirichlet distribution », janv. 2003.

[20]   « AVIRIS - Airborne Visible / Infrared Imaging Spectrometer ». https://aviris.jpl.nasa.gov/ (consulté le janv. 03, 2020).

.